

Quasi two-dimensional magnetism in spin- $\frac{1}{2}$ square lattice compound Cu[C₆H₂(COO)₄][H₃N-(CH₂)₂-NH₃] \cdot 3H₂O

S. Guchhait,¹ S. Baby,² M. Padmanabhan,³ A. Medhi,¹ and R. Nath^{1,*}

¹*School of Physics, Indian Institute of Science Education and Research Thiruvananthapuram-695551, Kerala, India*

²*Department of Chemistry, Christian College Chengannur, Alappuzha, Kerala-689122, India*

³*Department of Chemistry, Amrita Vishwa Vidyapeetham, Amritapuri, Kerala-690525, India*

(Dated: March 25, 2022)

We report the crystal growth and structural and magnetic properties of quasi two-dimensional $S = 1/2$ quantum magnet Cu[C₆H₂(COO)₄][H₃N-(CH₂)₂-NH₃] \cdot 3H₂O. It is found to crystallize in a monoclinic structure with space group $C2/m$. The CuO₄ plaquettes are connected into a two-dimensional framework in the ab -plane through the anions of [C₆H₂(COO)₄]⁴⁻ (pyromellitic acid). The [H₃N-(CH₂)₂-NH₃]²⁺ \cdot 3H₂O groups are located between the layers and provide a weak interlayer connection via hydrogen (H...O) bonds. The temperature dependent magnetic susceptibility is well described by $S = 1/2$ frustrated square lattice ($J_1 - J_2$) model with nearest-neighbor interaction $J_1/k_B \simeq 5.35$ K and next-nearest-neighbor interaction $J_2/k_B \simeq -0.01$ K. Even, our analysis using frustrated rectangular lattice ($J_{1a,b} - J_2$) model confirms almost isotropic nearest-neighbour interactions ($J_{1a}/k_B \simeq 5.31$ K and $J_{1b}/k_B \simeq 5.38$ K) in the ab -plane and $J_2/k_B \simeq -0.24$ K. Further, the isothermal magnetization at $T = 1.9$ K is also well described by a non-frustrated square lattice model with $J_1/k_B \simeq 5.2$ K. Based on the J_2/J_1 ratio, the compound can be placed in the Néel antiferromagnetic state of the $J_1 - J_2$ phase diagram. No signature of magnetic long-range-order was detected down to 2 K.

PACS numbers: 75.30.Et, 75.50.Ee, 75.40.Cx, 75.50.-y, 75.10.Jm

I. INTRODUCTION

Quasi-two-dimensional (2D) antiferromagnets are ideal materials to study the interplay between quantum fluctuations and magnetic frustration due to competing interactions. Frustrated square lattice (FSL or $J_1 - J_2$ model) model is the best known example in this category. The Hamiltonian of the isotropic FSL model can be written as

$$\hat{H} = J_1 \sum_{\langle ij \rangle_1} S_i \cdot S_j + J_2 \sum_{\langle ij \rangle_2} S_i \cdot S_j, \quad (1)$$

where J_1 and J_2 are the nearest-neighbour (NN) (along the edge) and next-nearest-neighbour (NNN) (along the diagonal) interactions, respectively in a square. The classically possible ground states in this model are determined by the frustration angle $\phi = \tan^{-1}(J_2/J_1)$. [1] There are three possible order states: Néel antiferromagnetic (NAF, $-0.5\pi \leq \phi \leq 0.15\pi$), columnar antiferromagnetic (CAF, $0.15\pi \leq \phi \leq 0.85\pi$), and ferromagnetic (FM, $0.85\pi \leq \phi \leq -0.5\pi$) states with wave vectors $(Q_x, Q_y) = (\pi, \pi)$, $[(\pi, 0)$ or $(0, \pi)]$, and $(0, 0)$, respectively. [2, 3] The transition regimes NAF/CAF and CAF/FM are known as quantum critical regimes, though the precise boundaries of these regimes are not yet well defined. It is proposed that the ground state in these critical regimes are not exactly quantum spin-liquid but different dimer phases with a singlet gap and gapless nematic phases, respectively. [2, 4–8]

The $J_1 - J_2$ phase diagram has been extended further to the spatially anisotropic square lattice or rectangular lattice (known as $J_{1a,b} - J_2$ model). [9] The Hamiltonian for a 2D $S = 1/2$ frustrated rectangular lattice (FRL) model can be written as

$$\hat{H} = J_{1a} \sum_{\langle ij \rangle_{1a}} S_i \cdot S_j + J_{1b} \sum_{\langle ij \rangle_{1b}} S_i \cdot S_j + J_2 \sum_{\langle ij \rangle_2} S_i \cdot S_j. \quad (2)$$

Here, J_{1a} and J_{1b} are the anisotropic exchange couplings along the edges of the square and the coupling along the diagonals (J_2) remains same. The classically predicted phase diagram becomes a function of frustration angle

$$\phi = \tan^{-1} \left(J_2 / \sqrt{\frac{J_{1a}^2 + J_{1b}^2}{2}} \right) \text{ and anisotropy parameter}$$

$\theta = \tan^{-1}(J_{1b}/J_{1a})$. The introduction of a rectangular distortion does not significantly change the phase diagram. The predicted phases are FM, NAF, and columnar antiferromagnets [CAF_a, $(Q_x, Q_y) = (\pi, 0)$ and CAF_b, $(Q_x, Q_y) = (0, \pi)$]. The only difference is that the CAF phases are degenerate for the isotropic model ($J_{1a} = J_{1b}$) with $\theta = \frac{\pi}{4}$ or $\theta = -\frac{3\pi}{4}$. Further, the $J_{1a,b} - J_2$ model predicts that the CAF phase is stable for all values of ϕ , especially in the spin nematic phase regime of the isotropic $J_1 - J_2$ model. [9]

The $S = 1/2$ FSL model has been realized in the class of layered V^{4+} based inorganic compounds $AA'(\text{VO})(\text{PO}_4)_2$ ($AA' = \text{Zn}_2, \text{Pb}_2, \text{SrZn}, \text{PbZn}, \text{BaZn}$, and BaCd) and $\text{Li}_2\text{VO}(\text{Si}, \text{Ge})\text{O}_4$. [10–20] Among these compounds, $\text{BaCdVO}(\text{PO}_4)_2$ is the one located very close to the nematic phase regime in the $J_1 - J_2$ phase diagram and is being extensively studied. Some of the recent studies have reported the signature of spin nematic

* rnath@iisertvm.ac.in

phase in $\text{BaCdVO}(\text{PO}_4)_2$. [21–23] A few metal-organic compounds based on V^{4+} and Cu^{2+} have also been studied in light of the 2D spin-1/2 Heisenberg model. [24–27] A series of Cu based quasi-2D organometallic magnets where Cu^{2+} ions are bridged by pyrazine molecules are $[\text{Cu}(\text{HF}_2)(\text{pyz})_2]X$ ($X = \text{BF}_4^-, \text{ClO}_4^-, \text{PF}_6^-, \text{SbF}_6^-,$ and AsF_6^-) [28] and $[\text{Cu}(\text{pyz})_2]X_2$ ($X = \text{ClO}_4^-$ and BF_4^-). [29–31] These compounds are having square lattice network with negligible NNN exchange coupling (J_2). Another family of Cu based organo-metallic square lattice compounds are $A_2\text{CuX}_4$ ($A = 5\text{CAP}$ and 5MAP , $X = \text{Br}$ and Cl) without frustration. [25] Recently, we have reported that $\text{Cu}[\text{C}_6\text{H}_2(\text{COO})_4][\text{C}_2\text{H}_5\text{NH}_3]_2$ is a quasi-2D spatially anisotropic non-frustrated spin-1/2 square lattice with exchange couplings $J_{1a}/k_B = 5.6$ K and $J_{1c}/k_B = 8.0$ K along a - and c -directions, respectively. [27]

In this work, we report the synthesis and magnetic properties of a new organic spin-1/2 quantum magnet $\text{Cu}[\text{C}_6\text{H}_2(\text{COO})_4][\text{H}_3\text{N}-(\text{CH}_2)_2-\text{NH}_3]\cdot 3\text{H}_2\text{O}$ (or $\text{C}_{12}\text{H}_{18}\text{CuN}_2\text{O}_{11}$). The magnetization data analysis confirms the non-frustrated quasi-2D nature with a weak anisotropy in the in-plane couplings. It does not show the onset of magnetic long-range-ordering (LRO) down to 2 K, reflecting weak inter-plane coupling and hence perfect two-dimensionality.

II. TECHNIQUES

Single crystals of the Cu(II)-based metal organic hybrid compound $\text{C}_{12}\text{H}_{18}\text{CuN}_2\text{O}_{11}$ were synthesised by using 1,2,4,5-benzenetetracarboxylic acid (H_4BTC). Since the compound contains four carboxylic acid groups, we were initially getting mixture of products from which isolation of pure phase of the material was difficult. After repeated trials and by varying the reaction conditions the phase-pure form of the compound was obtained by adopting the following procedure. Copper acetate monohydrate (5 mmol, 1.00 g), ethylene diamine (5 mmol, 0.35 mL), H_4BTC (5 mmol, 1.27 g) were reacted in 30 mL DMF-water mixture (taken in 1:1 volume ratio). The initial blue product formed was filtered out. The clear and pale blue filtrate obtained was kept for slow evaporation for 8 days at room temperature. Light bluish needle type crystals of the target compound in phase-pure form were separated and dried in air. The yield was 45% (based on Cu).

Single crystal x-ray diffraction (XRD) was performed on a good-quality single crystal at room temperature using a Bruker KAPPA APEX-II CCD diffractometer equipped with graphite monochromated Mo $K_{\alpha 1}$ radiation ($\lambda = 0.71073$ Å). The data were collected using APEX3 software and reduced with SAINT/XPREP. [32] An empirical absorption correction was done using the SADABS program. [33] The structure was solved with direct methods using SHELXT-2018/2 [34] and refined by the full matrix least squares on F^2 using SHELXL-2018/3, respectively. [35] All the hydrogen atoms were

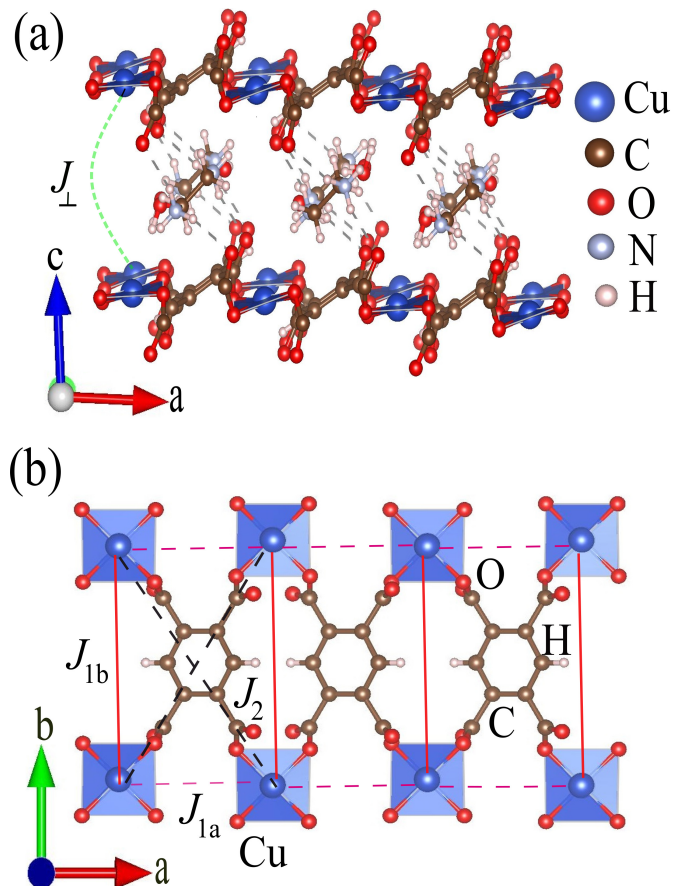


FIG. 1. (a) Three dimensional view of the $\text{C}_{12}\text{H}_{18}\text{CuN}_2\text{O}_{11}$ structure featuring negatively charged $\{\text{Cu}[\text{C}_6\text{H}_2(\text{COO})_4]\}^{2-}$ layers connected by the $[\text{H}_3\text{N}-(\text{CH}_2)_2-\text{NH}_3]^{2+}\cdot 3\text{H}_2\text{O}$ groups through hydrogen bond. J_{\perp} is the exchange coupling between two layer. (b) A section of the $\{\text{Cu}[\text{C}_6\text{H}_2(\text{COO})_4]\}^{2-}$ layer in ab -plane showing the exchange couplings forming a rectangular spin lattice of Cu^{2+} ions. The exchange couplings J_{1a} and J_{1b} are along the edges of the rectangle and J_2 is along the diagonal.

placed geometrically and held in the riding mode for the final refinements. The final refinements included atomic positions for all the atoms, anisotropic thermal parameters for all the nonhydrogen atoms, and isotropic thermal parameters for the hydrogen atoms. The crystal data and details of the structure refinement parameters are listed in Table I.

As the size of the crystals was too small, it was not possible to do the magnetic measurements on the individual crystals and hence powder sample was used for this purpose. The temperature (T) dependent magnetic susceptibility $[\chi(T)]$ in four different magnetic fields ($\mu_0 H = 0.5, 1, 3,$ and 5 T) was measured in the temperature range $2 \leq T \leq 300$ K using the vibrating sample magnetometer (VSM) attachment to the Physical Property Measurement System (PPMS, Quantum Design). A magnetic isotherm (magnetization M vs field H) was measured by varying the magnetic field from 0 to 14 T at $T = 1.9$ K.

TABLE I. Crystal structure data for $C_{12}H_{18}CuN_2O_{11}$ at room temperature.

Empirical formula	$C_{12}H_{18}CuN_2O_{11}$
Formula weight (M_r)	429.8
Temperature	296(2) K
Crystal system	Monoclinic
Space group	$C2/m$
Lattice parameters	$a = 11.4258(3) \text{ \AA}$, $b = 18.4562(5) \text{ \AA}$, $c = 7.4747(2) \text{ \AA}$, $\beta = 95.079(2)^\circ$
Unit cell volume (V_{cell})	$1570.05(7) \text{ \AA}^3$
Z	4
Radiation type	$MoK_{\alpha 1}$
Wavelength (λ)	0.71073 \AA
Diffractometer	Bruker KAPPA APEX-II CCD
Crystal size	$0.2 \times 0.15 \times 0.1 \text{ mm}^3$
2Θ range for data collection	4.2° to 50°
Index ranges	$-13 \leq h \leq 13$, $-21 \leq k \leq 21$, $-8 \leq l \leq 8$
Absorption coefficient (μ)	1.459 mm^{-1}
$F(000)$	884
Reflections collected	6671
Independent reflections	1429 [$R_{\text{int}} = 0.0183$]
Data/restraints/parameters	1429/3/128
Goodness-of-fit on F^2	1.104
Final R indexes, $I \geq 2\sigma(I)$	$R_1 = 0.0272$, $\omega R_2 = 0.0709$
Final R indexes, all data	$R_1 = 0.0293$, $\omega R_2 = 0.0723$
Largest difference peak/hole	$1.014 / -0.487 \text{ e.\AA}^{-3}$
Calculated crystal density ρ_{cal}	1.818 mg/mm^3

The Quantum Monte Carlo (QMC) simulation for magnetization was performed assuming the Heisenberg model on a nonfrustrated square lattice with an isotropic exchange coupling. We used the Hamiltonian in the presence of a magnetic field $\hat{H} = J \sum_{\langle i,j \rangle} S_i \cdot S_j - H \sum_i S_i^z$, where J represents the exchange coupling strength between spins at the i^{th} and j^{th} sites and H is the external magnetic field. We used the directed loop QMC algorithm in the stochastic series expansion representation[36, 37] implemented in the ALPS software package.[38] The lattice size was taken to be 20×20 (400 sites) and measurements were done from a simulation of about 10^5 sweeps including about 5000 thermalization sweeps.

III. RESULTS

A. Crystal Structure

$C_{12}H_{18}CuN_2O_{11}$ stabilizes in a monoclinic crystal structure with space group $C2/m$. The lattice parameters, atomic positions, and main bond distances along with their angles at room temperature are tabulated in Tables I, II, and III, respectively. The crystal structure is shown in Fig. 1. Each Cu atom is bonded with four O atoms forming a CuO_4 square. As the Cu-O distances are unequal, CuO_4 is slightly distorted. The CuO_4 plaquettes are connected via $[C_6H_2(COO)_4]^{4-}$ building rectangular layers in the ab -plane [Fig. 1(b)]. The distance between NN Cu^{2+} ions along the smaller edge (along a -axis) of a rectangle is $\sim 5.7176 \text{ \AA}$ while along the longer edge (along b -axis) these distances are unequal ($\sim 8.9963 \text{ \AA}$ and $\sim 9.4599 \text{ \AA}$). Hence, the rectangular lattice is expected to be anisotropic or to form a trapezoid. The corresponding exchange couplings are marked as J_{1a} and J_{1b} along the a - and b -axes, respectively as shown in Fig. 1(b). The NNN distances between Cu^{2+} ions along diagonals of the rectangle is $\sim 10.8533 \text{ \AA}$ with exchange coupling J_2 . Further, the distance between two Cu^{2+} ions in two adjacent layers along the crystallography c -axis is $\sim 7.4747 \text{ \AA}$. The $[H_3N-(CH_2)_2-NH_3]^{2+} \cdot 3H_2O$ groups lie sandwiched between the layers and are connecting the Cu^{2+} ions from the adjacent layers via weak hydrogen bonds [see Fig. 1(a)]. Thus, because of the large spacial distance and weak hydrogen bonding, the inter-layer interaction (J_{\perp}) is expected to be very weak.

B. Magnetic Susceptibility

Magnetic susceptibility ($\chi = M/H$) as a function of temperature (T) measured in an applied field of $\mu_0 H = 0.5 \text{ T}$ is shown in the upper panel of Fig. 2. In the high temperature region, $\chi(T)$ increases systematically with lowering temperature, typically expected in the paramagnetic state. It then passes through a broad maximum at around $T_{\chi}^{\text{max}} \simeq 5.13 \text{ K}$ mimicking the short-range AF ordering in the system. This is a clear evidence of quasi-2D nature of the compound. No signature of magnetic LRO was observed down to 2 K. As shown in the inset of the upper panel of Fig. 2, the broad maximum shifts towards lower temperatures with increasing magnetic field. This behavior is quite similar to that observed in other low-dimensional antiferromagnets.[10, 27]

$\chi(T)$ in the high temperature region can be fitted by

$$\chi(T) = \chi_0 + \frac{C}{T - \theta_{CW}}, \quad (3)$$

where, χ_0 is the temperature-independent susceptibility consisting of core diamagnetic susceptibility (χ_{dia}) of the core electron shells of the atoms and Van-Vleck

TABLE II. The atomic coordinates (x, y, z) for $C_{12}H_{18}CuN_2O_{11}$. U_{iso} is the isotropic atomic displacement parameters which is defined as one-third of the trace of the orthogonal U_{ij} tensor. The errors are from the least-square structure refinement. The positions of hydrogen atoms are fixed.

Atomic sites	x	y	z	$U_{iso}(\text{\AA}^2)$
Cu(1)	0.5000	0.2563(1)	0.5000	0.014(1)
C(1)	0.6438(2)	0.3652(1)	0.4217(3)	0.017(1)
C(2)	0.7105(2)	0.4346(1)	0.4625(3)	0.016(1)
C(3)	0.8186(2)	0.4346(1)	0.5676(3)	0.015(1)
C(4)	0.8826(2)	0.3647(1)	0.6121(3)	0.017(1)
C(5)	0.6582(3)	0.5000	0.4095(5)	0.018(1)
C(6)	0.8710(3)	0.5000	0.6194(5)	0.017(1)
C(7)	0.8001(3)	0.2579(2)	1.0704(4)	0.028(1)
N(1)	0.8215(2)	0.3372(1)	1.0812(3)	0.027(1)
O(1')	0.6135(3)	0.4228(2)	0.8964(3)	0.053(1)
O(2')	1.1385(14)	0.5000	0.9284(18)	0.276(7)
O(1)	0.6159(1)	0.3316(1)	0.5616(2)	0.019(1)
O(2)	0.6151(2)	0.3465(1)	0.2655(2)	0.029(1)
O(3)	0.8804(1)	0.3193(1)	0.4837(2)	0.021(1)
O(4)	0.9361(2)	0.3563(1)	0.7637(2)	0.026(1)
H(5)	0.5875	0.5000	0.3377	0.021
H(6)	0.9423	0.5000	0.6899	0.021
H(1A)	0.8805	0.3462	1.1641	0.04
H(1B)	0.8399	0.3534	0.9751	0.04
H(1C)	0.7569	0.3595	1.1109	0.04
H(7A)	0.7809	0.2399	1.1862	0.034
H(7B)	0.8706	0.2333	1.0394	0.034
H(1A')	0.581(3)	0.407(4)	0.784(4)	0.14(3)
H(1B')	0.6826	0.4369	0.8998	0.21(4)

TABLE III. Some selected bond lengths and bond angles for $C_{12}H_{18}CuN_2O_{11}$.

	Bond length (\AA)		Bond length (\AA)	
C(1)-O(2)	1.234(3)	C(4)-O(4)	1.249(3)	
C(1)-O(1)	1.280(3)	C(4)-O(3)	1.273(3)	
C(1)-C(2)	1.508(3)	N(1)-C(7)	1.485(4)	
C(2)-C(5)	1.389(3)	C(7)-C(7) ¹	1.513(5)	
C(2)-C(3)	1.404(3)	O(1)-Cu(1)	1.9464(16)	
C(3)-C(6)	1.388(3)	O(3)-Cu(1) ²	1.9490(16)	
C(3)-C(4)	1.505(3)			
	Bond angles ($^\circ$)		Bond angles ($^\circ$)	
O(2)-C(1)-O(1)	124.9(2)	C(2) ³ -C(5)-C(2)	120.7(3)	
O(2)-C(1)-C(2)	121.1(2)	C(3) ³ -C(6)-C(3)	121.0(3)	
O(1)-C(1)-C(2)	113.9(2)	N(1)-C(7)-C(7) ¹	109.8(3)	
C(5)-C(2)-C(3)	119.6(2)	C(1)-O(1)-Cu(1)	111.50(15)	
C(5)-C(2)-C(1)	118.9(2)	C(4)-O(3)-Cu(1) ²	117.21(15)	
C(3)-C(2)-C(1)	121.1(2)	O(1)-Cu(1)-O(1) ⁴	88.92(10)	
C(6)-C(3)-C(2)	119.5(2)	O(1)-Cu(1)-O(3) ⁵	169.86(7)	
C(6)-C(3)-C(4)	119.6(2)	O(1) ⁴ -Cu(1)-O(3) ⁵	92.14(7)	
C(2)-C(3)-C(4)	120.7(2)	O(1)-Cu(1)-O(3) ²	92.14(7)	
O(4)-C(4)-O(3)	125.2(2)	O(1) ⁴ -Cu(1)-O(3) ²	169.86(7)	
O(4)-C(4)-C(3)	119.8(2)	O(3) ⁵ -Cu(1)-O(3) ²	88.59(10)	
O(3)-C(4)-C(3)	114.9(2)			

Symmetry transformations used to generate equivalent atoms of table III:

$$\begin{aligned} &^1-x+3/2,-y+1/2,-z+2 \quad ^2-x+3/2,-y+1/2,-z+1 \quad ^3x,-y+1,z \\ &^4-x+1,y,-z+1 \quad ^5x-1/2,-y+1/2,z. \end{aligned}$$

dependent term

$$\chi(T) = \chi_0 + \chi_{\text{spin}}(T). \quad (4)$$

Here, $\chi_{\text{spin}}(T)$ is the high-temperature series expansion (HTSE) of spin susceptibility for the spin-1/2 FSL model ($J_1 - J_2$ model).[17, 42] The expression is given by

$$\chi_{\text{spin}}(T) = \frac{N_A g^2 \mu_B^2}{k_B T} \sum_n \left(\frac{J_1}{k_B T} \right)^n \sum_m c_{m,n} \left(\frac{J_2}{J_1} \right)^m \quad (5)$$

paramagnetic susceptibility (χ_{vV}) of the open shells of the Cu^{2+} ions in the sample. The second term is the Curie-Weiss (CW) law where C is Curie constant and θ_{CW} is Curie-Weiss temperature. Our experimental $\chi(T)$ data in the temperature range $T \geq 18$ K were fitted well by Eq. (3) yielding $\chi_0 \simeq -2.26 \times 10^{-4} \text{ cm}^3/\text{mol-Cu}^{2+}$, $C \simeq 0.46 \text{ cm}^3\cdot\text{K}/\text{mol-Cu}^{2+}$, and $\theta_{\text{CW}} \simeq -5.17$ K. The negative Curie-Weiss temperature indicates predominance of AF exchange interactions between the Cu^{2+} ions in the compound. From the value of C , the effective magnetic moment $\mu_{\text{eff}} = (3k_B C/N_A \mu_B^2)^{1/2}$, (where k_B is the Boltzmann constant, N_A is the Avogadro number, and μ_B is the Bohr magneton) is estimated to be $\mu_{\text{eff}} \simeq 1.91 \mu_B/\text{Cu}^{2+}$. This value of μ_{eff} [= $g\sqrt{S(S+1)}\mu_B$] corresponds to a Land g -factor of $g \simeq 2.21$ which is slightly larger than the ideal value ($g = 2$), expected for spin-1/2. A slightly larger value of g is typically found for Cu^{2+} based compounds from ESR experiments.[39–41]

To understand the geometry of the spin lattice, $\chi(T)$ in the high temperature regime was fitted by the sum of a temperature independent term (χ_0) and a temperature

The values of the coefficients, $c_{m,n}$ are tabulated in Ref. [17]. The best fit of the $\chi(T)$ data (upper panel of Fig. 2) by Eq. (4) in the temperature range $T > 5.4$ K resulted two different solutions: Solution I: $\chi_0 \simeq -2.65 \times 10^{-4} \text{ cm}^3/\text{mol-Cu}^{2+}$, $J_1/k_B \simeq 5.35$ K, $J_2/k_B \simeq -0.01$ K, and $g \simeq 2.23$ and Solution II: $\chi_0 \simeq -2.68 \times 10^{-4} \text{ cm}^3/\text{mol-Cu}^{2+}$, $J_1/k_B \simeq 5.35$ K, $J_2/k_B \simeq 0.01$ K, and $g \simeq 2.23$. As discussed later, the solution I appears to be the correct solution. In both cases, the value of J_2 is negligibly small and hence can be ignored. Nevertheless, for both the solutions the compound can be placed in the NAF regime of the $J_1 - J_2$ phase diagram.

As discussed earlier, the Cu^{2+} ions form a slightly distorted square lattice. In an attempt to test the spin-lattice, $\chi(T)$ data were fitted by the FRL model (see

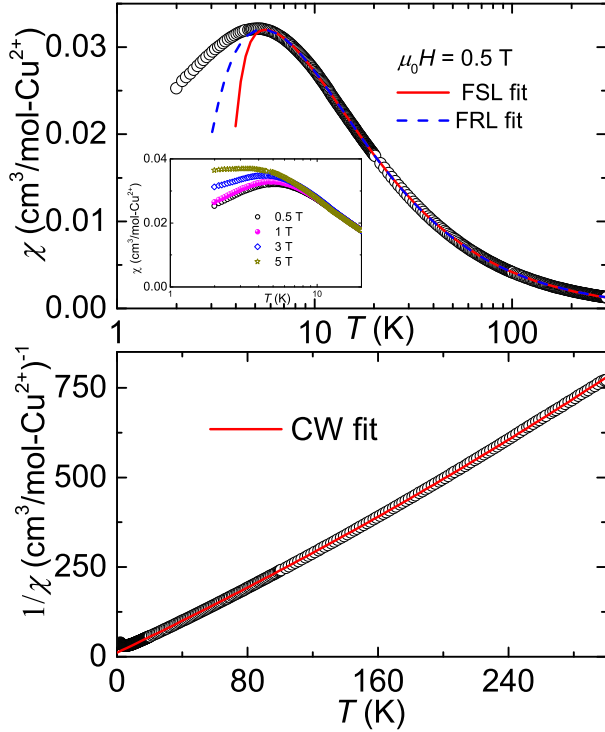


FIG. 2. Upper panel: $\chi(T)$ vs T in an applied field of $\mu_0 H = 0.5$ T. The solid and dashed lines are the best fits of the data using HTSE of frustrated square lattice and frustrated rectangular lattice models [Eq. (4)], respectively. Inset: The low temperature $\chi(T)$ measured in different fields. Lower panel: Inverse magnetic susceptibility ($1/\chi$) vs T and the solid line is the Curie-Weiss fit.

Fig. 2). The fit was done using Eq. (4) where χ_{spin} is taken as HTSE for the anisotropic FSL/FRL model given in Ref. [42]. Our fit in the temperature range $T > 5.4$ K results $\chi_0 \simeq -2.3 \times 10^{-4}$ cm³/mol-Cu²⁺, $g \simeq 2.22$, $J_{1a}/k_B \simeq 5.31$ K, $J_{1b}/k_B \simeq 5.38$ K, and $J_2/k_B \simeq -0.24$ K. As J_{1a}/k_B and J_{1b}/k_B are having almost equal magnitude, the spin-lattice can essentially be treated as a weakly anisotropic square lattice.

C. Magnetic Isotherm

Magnetization (M) as a function of applied field (H) measured at $T = 1.9$ K is shown in Fig. 3. M varies almost linearly with H with a small curvature and at $\mu_0 H = 14$ T it is still below the saturation field. According to theoretical calculation by Schmidt *et al.*[7], the saturation field of a FSL model can be expressed as

$$\mu_0 H_S = \frac{J_c k_B z S}{g \mu_B} \left\{ \left[1 - \frac{1}{2} (\cos Q_x + \cos Q_y) \right] \cos \phi + (1 - \cos Q_x \cos Q_y) \sin \phi \right\}, \quad (6)$$

where $z = 4$ is the magnetic coordination number, $S = 1/2$, and (Q_x, Q_y) are the wave vectors which are dif-

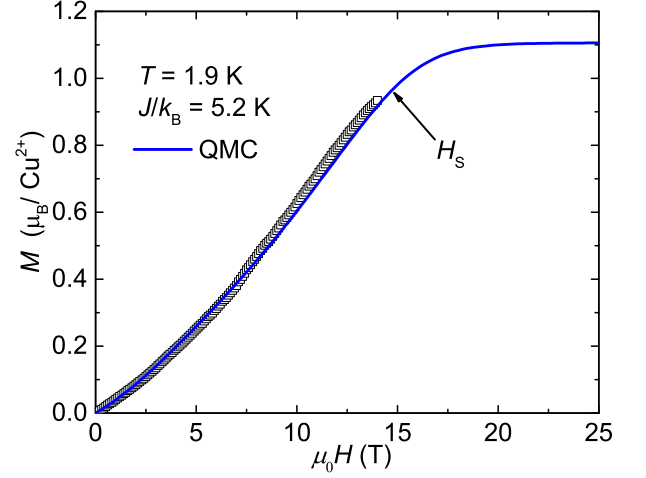


FIG. 3. Magnetization (M) as a function of magnetic field H at $T = 1.9$ K measured up to 14 T. The solid line is the QMC simulation, assuming a uniform nonfrustrated square lattice model with $J/k_B = 5.2$ K.

ferent for different ordered states. Putting $(Q_x, Q_y) = (\pi, \pi)$, the saturation field for the NAF phase will have the form $\mu_0 H_S = 4J_1 k_B / (g \mu_B)$, which is independent of J_2 . Using $J_1/k_B \simeq 5.35$ K and $g = 2.23$ in this formula, the value of saturation field is calculated to be $\mu_0 H_S^{\text{sq}} \simeq 14.3$ T. Even putting the values of J_{1a} and J_{1b} in a spin-1/2 FRL model, the saturation field is calculated to be $\mu_0 H_S^{\text{rect}} = 2(J_{1a} + J_{1b})k_B / (g \mu_B) \simeq 14.3$ T.[27]

In order to further understand the nature of spin lattice, QMC simulation is done taking $J/k_B = 5.2$ K in a non-frustrated square lattice model. As shown in Fig. 3, the QMC simulated data reproduce the shape of our experimental curve perfectly reflecting the non-frustrated square lattice nature of the spin-lattice. The simulated curve changes the slope at around $\mu_0 H \simeq 15$ T, which is very close to the saturation field expected for the compound. It reaches a saturation magnetization of $M_S \simeq 1.1 \mu_B / \text{Cu}^{2+}$ for $\mu_0 H > 15$ T which is consistent with the expected value of $M_S = gS \mu_B \simeq 1.1 \mu_B / \text{Cu}^{2+}$ for $S = 1/2$ and $g = 2.23$.

IV. DISCUSSION AND SUMMARY

According to mean field approximation, for the FSL model, one can write $\theta_{\text{CW}} = \frac{zS(S+1)}{3k_B} (J_1 + J_2)$. [43] Taking $S = 1/2$, $z = 4$, $J_1/k_B \simeq 5.35$ K, and $J_2/k_B \simeq -0.01$ K, we got $\theta_{\text{CW}} \simeq 5.34$ K which is very close to the CW temperature obtained from the $1/\chi$ analysis. Using the values of J_1 and J_2 , the frustration control parameter is calculated to be $\phi = -0.1^\circ$ ($\sim -0.0006\pi$), which places the compound in the NAF ordered state of the $J_1 - J_2$ phase diagram.[10] Similarly, for a FRL model one can write $\theta_{\text{CW}} = \frac{(J_{1a} + J_{1b}) + J_2}{2} / k_B$. Taking $J_{1a}/k_B \simeq 5.31$ K, $J_{1b}/k_B \simeq 5.38$ K, and $J_2/k_B \simeq -0.24$ K we got $\theta_{\text{CW}} \simeq$

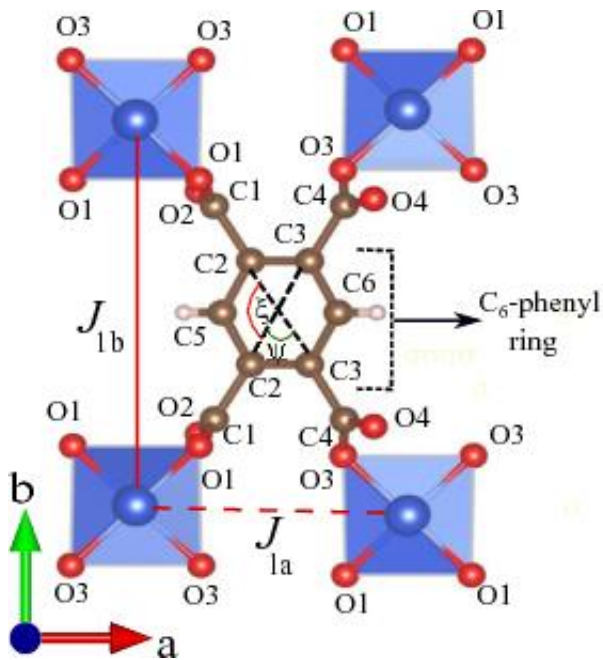


FIG. 4.

A rectangular unit showing the superexchange interactions J_{1a} and J_{1b} along with their respective bridging angles $\angle\psi \simeq 60.5^\circ$ and $\angle\xi \simeq 119.6^\circ$ between C-atoms, in the C_6 -phenyl ring.

5.11 K which is even closer to the CW temperature obtained from the $1/\chi$ analysis. The anisotropic angle and frustration angle are estimated to be $\theta \simeq 0.252\pi$ and $\phi \simeq -0.014\pi$, respectively in the NAF regime of the $J_{1a,b} - J_2$ phase diagram.[9]

Usually, in a frustrated magnet, the extent of frustration can be quantified by the frustration parameter $f = \frac{|\theta_{CW}|}{T_N}$. $C_{12}H_{18}CuN_2O_{11}$ has no magnetic LRO down to 2 K which makes this system a good example of a quasi-2D AF system. The lower limit of the frustration parameter of this compound is estimated to be $f > \frac{5.17}{2} \simeq 2.6$, taking the upper limit of $T_N = 2$ K. Here, $|\theta_{CW}| > T_N$ implies that the magnetic LRO (T_N) is prevented by quantum fluctuations due to low dimensionality of the spin-lattice and the role of frustration has negligible effect. Further, assuming that $T_N < 2$ K and using the appropriate exchange couplings, the upper limit of the inter-layer coupling is estimated to be negligibly small compared to the intra-layer coupling.[3, 44] Thus, this compound is another example of a quasi-2D nonfrustrated system with $J_1/T_N > 2.67$, similar to the compounds tabulated in Ref. [24].

From the crystal structure, the Cu-Cu distance along b -direction is greater than the one along a -

direction. Therefore, one would expect J_{1a} to be larger than J_{1b} . Similar scenario has been realized in $Cu[C_6H_2(COO)_4][C_2H_5NH_3]_2$ in which the DFT calculations show that $J_{1a} < J_{1c}$, even though the Cu-Cu distance along a -direction is almost half of the distance along c -direction.[27] This non-trivial behaviour is attributed to the characteristic features of $[C_6H_2(COO)_4]^{4-}$ anion through which the superexchange takes place. In $Cu[C_6H_2(COO)_4][C_2H_5NH_3]_2$, the effective bridging angles between C atoms belonging to the C_6 -phenyl ring along the superexchange paths are $\angle\psi \simeq 59.9^\circ$ and $\angle\xi \simeq 120.1^\circ$ for J_{1a} and J_{1c} , respectively in the ac -plane. Therefore, it is argued that according to Goodenough-Kanamori-Anderson rules one finds $J_{1c} > J_{1a}$ and does not follow Cu-Cu distance. As shown in Fig. 4, in $C_{12}H_{18}CuN_2O_{11}$, the angles are $\angle\psi \simeq 60.5^\circ$ and $\angle\xi \simeq 119.6^\circ$. This explains why J_{1a} and J_{1b} have nearly equal values despite different Cu-Cu distances. However, to establish this proposition, a precise estimation of exchange couplings using band structure calculation is required.

In summary, we have synthesized single crystals of $C_{12}H_{18}CuN_2O_{11}$ and reported its crystal structure and magnetic properties in detail. $C_{12}H_{18}CuN_2O_{11}$ crystallizes in a monoclinic crystal structure with space group $C2/m$. Because of the low symmetry crystal structure, Cu^{2+} ions form anisotropic square lattices. The analysis of $\chi(T)$ demonstrates that the compound behaves as a nearly nonfrustrated spin-1/2 square lattice with $J_1/k_B \simeq 5.3$ K, despite its anisotropic (or rectangular) structural arrangement. Further, the shape of the magnetic isotherm at $T = 1.9$ K could be reproduced well by the QMC simulation assuming a non-frustrated square lattice with $J/k_B = 5.2$ K, supporting the $\chi(T)$ analysis. No sign of magnetic LRO down to 2 K indicates minuscule inter-plane coupling in the system. In this compound J_2 is negligibly small, but its strength can be increased and the frustration ratio J_2/J_1 can be tuned by an appropriate choice of the organic ligand that provides superexchange pathway between the magnetic ions. Thus, the metal organic complexes can reciprocate the inorganic compounds as the model systems in the $J_1 - J_2$ phase diagram.

V. ACKNOWLEDGEMENT

SG and RN acknowledge SERB, India for financial support bearing sanction order no. CRG/2019/000960. We thank Alex Andrews for his help in solving the crystal structure.

[1] N. Shannon, B. Schmidt, K. Penc, and P. Thalmeier, "Finite temperature properties and frustrated ferromag-

netism in a square lattice Heisenberg model," *Eur. Phys. J. B* **38**, 599 (2004).

- [2] N. Shannon, T. Momoi, and P. Sindzingre, “Nematic order in square lattice frustrated ferromagnets,” *Phys. Rev. Lett.* **96**, 027213 (2006).
- [3] B. Schmidt and P. Thalmeier, “Néel temperature and reentrant H - T phase diagram of quasi-two-dimensional frustrated magnets,” *Phys. Rev. B* **96**, 214443 (2017).
- [4] O. P. Sushkov, J. Oitmaa, and Z. Weihong, “Quantum phase transitions in the two-dimensional $J_1 - J_2$ model,” *Phys. Rev. B* **63**, 104420 (2001).
- [5] R. R. P. Singh, Z. Weihong, C. J. Hamer, and J. Oitmaa, “Dimer order with striped correlations in the $J_1 - J_2$ Heisenberg model,” *Phys. Rev. B* **60**, 7278 (1999).
- [6] L. Capriotti, F. Becca, A. Parola, and S. Sorella, “Suppression of dimer correlations in the two-dimensional $J_1 - J_2$ Heisenberg model: An exact diagonalization study,” *Phys. Rev. B* **67**, 212402 (2003).
- [7] B. Schmidt, P. Thalmeier, and N. Shannon, “Magneto-thermal effect in the frustrated square lattice $J_1 - J_2$ model,” *Phys. Rev. B* **76**, 125113 (2007).
- [8] B. Schmidt, N. Shannon, and P. Thalmeier, “The frustrated $J_1 - J_2$ model in high magnetic fields,” *J. Phys.: Condens. Matter* **19**, 145211 (2007).
- [9] B. Schmidt, M. Siahatgar, and P. Thalmeier, “Ordered moment in the anisotropic and frustrated square lattice Heisenberg model,” *Phys. Rev. B* **83**, 075123 (2011).
- [10] R. Nath, A. A. Tsirlin, H. Rosner, and C. Geibel, “Magnetic properties of $\text{BaCdVO}(\text{PO}_4)_2$: A strongly frustrated spin- $\frac{1}{2}$ square lattice close to the quantum critical regime,” *Phys. Rev. B* **78**, 064422 (2008).
- [11] R. Nath, Y. Furukawa, F. Borsa, E. E. Kaul, M. Baenitz, C. Geibel, and D. C. Johnston, “Single-crystal ^{31}P NMR studies of the frustrated square-lattice compound $\text{Pb}_2\text{VO}(\text{PO}_4)_2$,” *Phys. Rev. B* **80**, 214430 (2009).
- [12] A. Yogi, N. Ahmed, R. Nath, A. A. Tsirlin, S. Kundu, A. V. Mahajan, J. Sichelschmidt, B. Roy, and Y. Furukawa, “Antiferromagnetism of $\text{Zn}_2\text{VO}(\text{PO}_4)_2$,” *Phys. Rev. B* **91**, 024413 (2015).
- [13] A. A. Tsirlin, R. Nath, A. M. Abakumov, R. V. Shpanchenko, C. Geibel, and H. Rosner, “Frustrated square lattice with spatial anisotropy: Crystal structure and magnetic properties of $\text{PbZnVO}(\text{PO}_4)_2$,” *Phys. Rev. B* **81**, 174424 (2010).
- [14] P. Carretta, M. Filibian, R. Nath, C. Geibel, and P. J. C. King, “Fluctuations and correlations in a frustrated $S = \frac{1}{2}$ square lattice with competing ferromagnetic and antiferromagnetic interactions studied by muon-spin relaxation,” *Phys. Rev. B* **79**, 224432 (2009).
- [15] L. Bossoni, P. Carretta, R. Nath, M. Moscardini, M. Baenitz, and C. Geibel, “NMR and μSR study of spin correlations in $\text{SrZnVO}(\text{PO}_4)_2$: An $S = \frac{1}{2}$ frustrated magnet on a square lattice,” *Phys. Rev. B* **83**, 014412 (2011).
- [16] B. Roy, Y. Furukawa, R. Nath, and D. C. Johnston, “Low-temperature ^{31}P NMR study of the two-dimensional frustrated square lattice compound $\text{BaCdVO}(\text{PO}_4)_2$,” *J. Phys.: Conf. Ser.* **320**, 012048 (2011).
- [17] H. Rosner, R. R. P. Singh, W. H. Zheng, J. Oitmaa, and W. E. Pickett, “High-temperature expansions for the $J_1 - J_2$ Heisenberg models: Applications to ab initio calculated models for $\text{Li}_2\text{VOSiO}_4$ and $\text{Li}_2\text{VOGeO}_4$,” *Phys. Rev. B* **67**, 014416 (2003).
- [18] S. Bettler, F. Landolt, Ö. M. Aksoy, Z. Yan, S. Gvasaliya, Y. Qiu, E. Ressouche, K. Beauvois, S. Raymond, A. N. Ponomaryov, S. A. Zvyagin, and A. Zheludev, “Magnetic structure and spin waves in the frustrated ferro-antiferromagnet $\text{Pb}_2\text{VO}(\text{PO}_4)_2$,” *Phys. Rev. B* **99**, 184437 (2019).
- [19] A. A. Tsirlin, R. Nath, A. M. Abakumov, Y. Furukawa, D. C. Johnston, M. Hemmida, H.-A. Krug von Nidda, A. Loidl, C. Geibel, and H. Rosner, “Phase separation and frustrated square lattice magnetism of $\text{Na}_{1.5}\text{VOPO}_4\text{F}_{0.5}$,” *Phys. Rev. B* **84**, 014429 (2011).
- [20] A. A. Tsirlin, B. Schmidt, Y. Skourski, R. Nath, C. Geibel, and H. Rosner, “Exploring the spin- $\frac{1}{2}$ frustrated square lattice model with high-field magnetization studies,” *Phys. Rev. B* **80**, 132407 (2009).
- [21] K. Y. Povarov, V. K. Bhartiya, Z. Yan, and A. Zheludev, “Thermodynamics of a frustrated quantum magnet on a square lattice,” *Phys. Rev. B* **99**, 024413 (2019).
- [22] M. Skoulatos, F. Rucker, G. J. Nilsen, A. Bertin, E. Pomjakushina, J. Ollivier, A. Schneidewind, R. Georgii, O. Zaharko, L. Keller, C. Rüegg, C. Pfleiderer, B. Schmidt, N. Shannon, A. Kriele, A. Senyshyn, and A. Smerald, “Putative spin-nematic phase in $\text{BaCdVO}(\text{PO}_4)_2$,” *Phys. Rev. B* **100**, 014405 (2019).
- [23] V. K. Bhartiya, K. Y. Povarov, D. Blosser, S. Bettler, Z. Yan, S. Gvasaliya, S. Raymond, E. Ressouche, K. Beauvois, J. Xu, F. Yokaichiya, and A. Zheludev, “Presaturation phase with no dipolar order in a quantum ferro-antiferromagnet,” *Phys. Rev. Research* **1**, 033078 (2019).
- [24] S. Guchhait, U. Arjun, P. K. Anjana, M. Sahoo, A. Thirumurugan, A. Medhi, Y. Skourski, B. Koo, J. Sichelschmidt, B. Schmidt, M. Baenitz, and R. Nath, “Case study of bilayered spin- $\frac{1}{2}$ square lattice compound $\text{VO}(\text{HCOO})_2 \cdot \text{H}_2\text{O}$,” *Phys. Rev. Mater.* **3**, 104409 (2019).
- [25] F. M. Woodward, A. S. Albrecht, C. M. Wynn, C. P. Landee, and M. M. Turnbull, “Two-dimensional $S = \frac{1}{2}$ Heisenberg antiferromagnets: Synthesis, structure, and magnetic properties,” *Phys. Rev. B* **65**, 144412 (2002).
- [26] H. M. Rønnow, D. F. McMorrow, R. Coldea, A. Harrison, I. D. Youngson, T. G. Perring, G. Aeppli, O. Syljuåsen, K. Lefmann, and C. Rischel, “Spin Dynamics of the 2D Spin $\frac{1}{2}$ Quantum Antiferromagnet Copper Deuterioformate Tetradeuterate (CFTD),” *Phys. Rev. Lett.* **87**, 037202 (2001).
- [27] R. Nath, M. Padmanabhan, S. Baby, A. Thirumurugan, D. Ehlers, M. Hemmida, H.-A. Krug von Nidda, and A. A. Tsirlin, “Quasi-two-dimensional $S = \frac{1}{2}$ magnetism of $\text{Cu}[\text{C}_6\text{H}_2(\text{COO})_4][\text{C}_2\text{H}_5\text{NH}_3]_2$,” *Phys. Rev. B* **91**, 054409 (2015).
- [28] P. A. Goddard, J. Singleton, P. Sengupta, R. D. McDonald, T. Lancaster, S. J. Blundell, F. L. Pratt, S. Cox, N. Harrison, J. L. Manson, H. I. Southerland, and J. A. Schlueter, “Experimentally determining the exchange parameters of quasi-two-dimensional Heisenberg magnets,” *New J. Phys.* **10**, 083025 (2008).
- [29] T. Lancaster, S. J. Blundell, M. L. Brooks, P. J. Baker, F. L. Pratt, J. L. Manson, M. M. Conner, F. Xiao, C. P. Landee, F. A. Chaves, S. Soriano, M. A. Novak, T. P. Papageorgiou, A. D. Bianchi, T. Herrmannsdörfer, J. Wosnitzer, and J. A. Schlueter, “Magnetic order in the $S = 1/2$ two-dimensional molecular antiferromagnet copper pyrazine perchlorate $\text{Cu}(\text{Pz})_2(\text{ClO}_4)_2$,” *Phys. Rev. B* **75**, 094421 (2007).

- [30] F. M. Woodward, P. J. Gibson, G. B. Jameson, C. P. Landee, M. M. Turnbull, and R. D. Willett, “Two-Dimensional Heisenberg Antiferromagnets: Syntheses, X-ray Structures, and Magnetic Behavior of $[\text{Cu}(\text{pz})_2](\text{ClO}_4)_2$, $[\text{Cu}(\text{pz})_2](\text{BF}_4)_2$, and $[\text{Cu}(\text{pz})_2(\text{NO}_3)](\text{PF}_6)$,” *Inorg. Chem.* **46**, 4256 (2007).
- [31] N. Tsyrlin, F. Xiao, A. Schneidewind, P. Link, H. M. Rønnow, J. Gavilano, C. P. Landee, M. M. Turnbull, and M. Kenzelmann, “Two-dimensional square-lattice $S = \frac{1}{2}$ antiferromagnet $\text{Cu}(\text{pz})_2(\text{ClO}_4)_2$,” *Phys. Rev. B* **81**, 134409 (2010).
- [32] A. Bruker, “APEX3, SAINT-Plus, XPREP,” (2016).
- [33] G. M. Sheldrick, “Siemens area correction absorption correction program,” University of Göttingen, Göttingen, Germany (1994).
- [34] G. M. Sheldrick, “Shelxt-integrated space-group and crystal-structure determination,” *Acta Crystallogr. A: Foundations and Advances* **71**, 3 (2015).
- [35] G. M. Sheldrick, “Shelxl-2018/3 software package,” University of Göttingen, Germany (2018).
- [36] A. W. Sandvik, “Stochastic series expansion method with operator-loop update,” *Phys. Rev. B* **59**, R14157 (1999).
- [37] F. Alet, S. Wessel, and M. Troyer, “Generalized directed loop method for quantum Monte Carlo simulations,” *Phys. Rev. E* **71**, 036706 (2005).
- [38] “ALPS project,” <http://alps.comp-phys.org/>.
- [39] R. Nath, K. M. Ranjith, J. Sichelschmidt, M. Baenitz, Y. Skourski, F. Alet, I. Rousochatzakis, and A. A. Tsirlin, “Hindered magnetic order from mixed dimensionalities in CuP_2O_6 ,” *Phys. Rev. B* **89**, 014407 (2014).
- [40] O. Janson, A. A. Tsirlin, J. Sichelschmidt, Y. Skourski, F. Weickert, and H. Rosner, “Long-range superexchange in $\text{Cu}_2\text{A}_2\text{O}_7$ ($A = \text{P}, \text{As}, \text{and V}$) as a key element of the microscopic magnetic model,” *Phys. Rev. B* **83**, 094435 (2011).
- [41] Y. C. Arango, E. Vavilova, M. Abdel-Hafiez, O. Janson, A. A. Tsirlin, H. Rosner, S.-L. Drechsler, M. Weil, G. Nénert, R. Klingeler, O. Volkova, A. Vasiliev, V. Kataev, and B. Büchner, “Magnetic properties of the low-dimensional spin- $\frac{1}{2}$ magnet $\alpha\text{-Cu}_2\text{As}_2\text{O}_7$,” *Phys. Rev. B* **84**, 134430 (2011).
- [42] H.-J. Schmidt, A. Lohmann, and J. Richter, “Eighth-order high-temperature expansion for general Heisenberg Hamiltonians,” *Phys. Rev. B* **84**, 104443 (2011).
- [43] C. Domb, , and A. R. Miedema, *Progress in Low Temperature Physics*, Vol. 4 (North Holland, Amsterdam, 1964).
- [44] N. Majlis, S. Selzer, and G. C. Strinati, “Dimensional crossover in the magnetic properties of highly anisotropic antiferromagnets,” *Phys. Rev. B* **45**, 7872 (1992).